Low-temperature thermal conductivity of antiferromagnetic $MnCl_2 \cdot 4H_2O$

G. S. Dixon
Oklahoma State University, Stillwater, Oklahoma 74074

V. Benedict and J. E. Rives
University of Georgia, Athens, Georgia 30602

(Received 3 January 1979)

Measurements of the thermal conductivity of $MnCl_2 \cdot 4H_2O$ as a function of temperature and magnetic field along the easy axis for sublattice magnetization are reported. Results are obtained in the antiferromagnetic, spin-flop, and paramagnetic phases. The principal features of the data can be ascribed to intrinsic scattering processes and reproduced by a simple model for two-magnon–one-phonon scattering. Inclusion of magnetic field dependence of the interaction-matrix elements is essential to the agreement between model and experiment.

I. INTRODUCTION

The antiferromagnet $MnCl_2 \cdot 4H_2O$ has received much attention as a model system for the study of the bulk properties of antiferromagnets.[1–19] Interest in this material has stemmed from the relatively low exchange and anisotropy energies, allowing the field-induced phases to be readily studied. In addition large, high-quality, single crystals can readily be prepared by solution growth. This feature is especially important for transport studies.

$MnCl_2 \cdot 4H_2O$ has a monoclinic structure with four Mn^{2+} ions per unit cell.[20–26] The magnetic structure has been determined by neutron diffraction to be collinear antiferromagnetic structure with the spin direction inclined from the normal to the a-b plane (c^* axis) by 2.8° toward the a axis.[27] At sufficiently low temperatures in magnetic fields along this direction the compound exhibits a first-order phase transition to a spin-flop phase at an internal field of $H_{AF} = 7.0$ kOe and a transition to the paramagnetic phase at $H_{FP} = 18.5$ kOe.[16] Figure 1 shows the magnetic unit cell for $MnCl_2 \cdot 4H_2O$. One notes that the magnetic unit cell is identical to the chemical unit cell in all three magnetic phases. It is also significant that each spin has parallel as well as antiparallel near neighbors. Thus, there are ferromagnetic contributions to the exchange energy as well as antiferromagnetic.

The anitferromagnetic contribution to the exchange energy and the anisotropy energy can be calculated from the measured critical fields for the magnetic phase boundaries.[16] The effective total exchange energy has been estimated from zero-field specific-heat measurements[8] to be $z_{eff}J_{eff}/k_B = +0.76$ K with $H_{ex} = +J\sum_{\langle ij\rangle}\vec{S}_i \cdot \vec{S}_j$ where the sum is over z_{eff} neighbors. This value is 25% larger than that obtained from the critical fields. This is to be expected since J_{eff} includes both the ferromagnetic and antiferromagnetic interactions indicated by the magnetic structure. The effect of the ferromagnetic interactions is to increase the energies of short-wavelength magnons. J_{eff} determines the width of the magnon energy band and thus, sets energy-conservation limits on magnon-phonon scattering processes. The anisotropy arises primarily from single-ion crystal-field effects.[16]

Previous reports of the thermal conductivity of $MnCl_2 \cdot 4H_2O$ have shown it to be a promising ma-

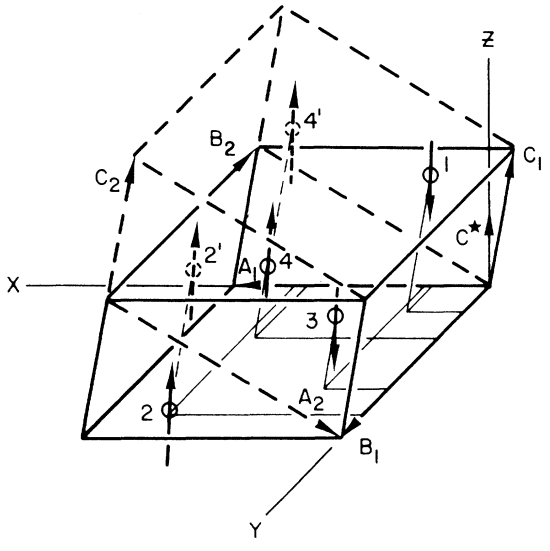

FIG. 1. Magnetic structure of $MnCl_2 \cdot 4H_2O$. Note that Mn^{2+} ions lie at general fourfold positions in this cell. Of the six nearest neighbors of each Mn^{2+} ion, four are aligned ferromagnetically; and two, antiferromagnetically. The unit cell used in this work and due to Groth (Ref. 20) is defined by the crystallographic axes A_1, B_2, C_1 and is shown by solid lines. The unit cell shown by the dashed lines (Ref. 21) is defined by the crystallographic axes A_2, B_2, C_2.

terial for a detailed investigation of the role of magnons in reducing the lattice thermal conductivity.[17–19] The magnons seem to be unimportant as heat carriers, and there is little, if any, effect from critical fluctuations near the Néel temperature, $T_N = 1.62$ K. In a saturating magnetic field, the lattice thermal conductivity closely approaches the ideal Casimir limit.

In Secs. II and III we present measurements of the thermal conductivity of $MnCl_2 \cdot 4H_2O$ as a function of temperature and magnetic fields applied along the easy axis for sublattice magnetization. These results are interpreted in terms of a simple model for two-magnon–one-phonon scattering presented in the preceding paper.[28]

II. EXPERIMENTAL

Single crystals of $MnCl_2 \cdot 4H_2O$ were grown from an aqueous solution by evaporation at ambient temperature. Samples in the shape of rectangular parallelepipids with dimensions of $4 \times 5 \times 25$ mm^3 were cut with a string saw so that the long dimension was parallel to the c^* crystallographic axis. These were coated with a thin layer of GE 7031 varnish to prevent the loss or absorption of water.

Thermal conductivities were measured by the steady-state longitudinal heat-flow method in a ^{3}He-evaporation refrigerator. Magnetic fields up to 40 kOe were applied along the c^* axis, parallel to the heat flow, by a superconducting solenoid. Nominal 470-Ω, 0.5-W Speer carbon resistors were used for thermometers. Details of the calibration and corrections for magnetoresistance were as described previously.[29]

III. RESULTS AND DISCUSSION

A. Experimental observations

Thermal conductivities were measured as a function of temperature in zero field and an applied field of 40 kOe from 0.25 to 2.7 K. Results were similar for all the samples studied. Figure 2 shows representative data for a sample in which a 14-mm thermometer separation was used. To facilitate intercomparison of results, all data shown in the figures are from this sample.

There are three effects of the magnetism in this compound that one might expect to observe in the thermal conductivity: heat conduction by the magnons, decreased lattice thermal conductivity due to critical fluctuation near T_N, and decreased lattice thermal conductivity due to scattering of phonons by magnons. Comparison of the zero-field and high-field data shows that the last of these is dominant in $MnCl_2 \cdot 4H_2O$. There is no significant difference in the thermal conductivity near $T_N = 1.62$ K. This shows that critical fluctuations have a negligible influence on the thermal conductivity since no phase transition occurs in a field of 40 kOe. At lower temperatures the high-field thermal conductivity exceeds that in zero field. Since the effect of the field is to depopulate the magnon branches by increasing their energy, this shows that scattering of phonons by magnons dominates any possible heat transport by the magnons in this temperature range. These features suggest $MnCl_2 \cdot 4H_2O$ as a system for testing models of magnon-phonon scattering processes.

To investigate the behavior of the thermal conductivity in the high-field phases, measurements were made as a function of magnetic field along representative isotherms. These are shown in Fig. 3. One

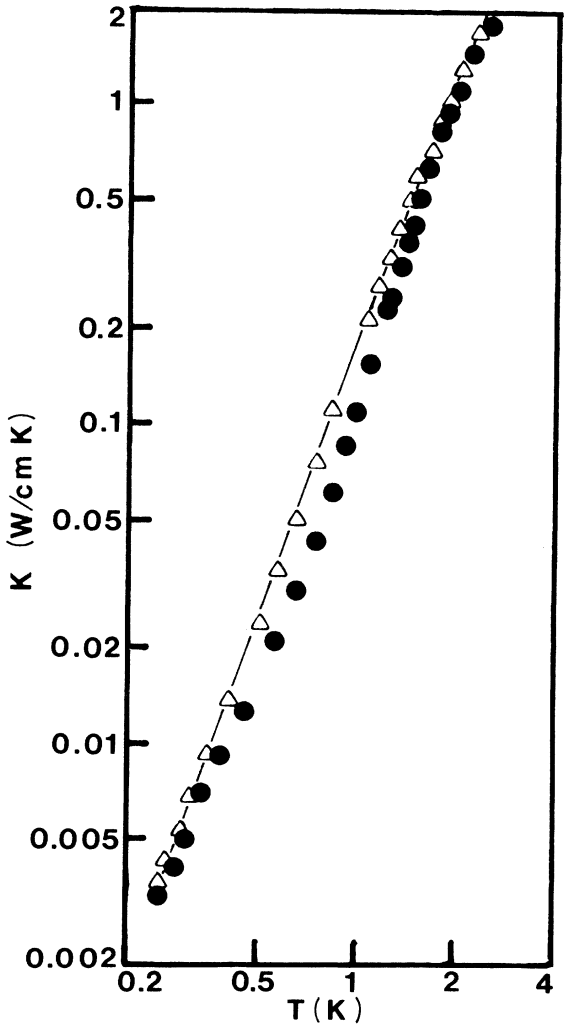

FIG. 2. Thermal conductivity of $MnCl_2 \cdot 4H_2O$ along the c^* axis. Filled circles are data in zero applied field. Triangles are data in a field of 40 kOe applied parallel to the c^* axis. The curve is a least-squares fit to the 40 kOe data as described in the text.

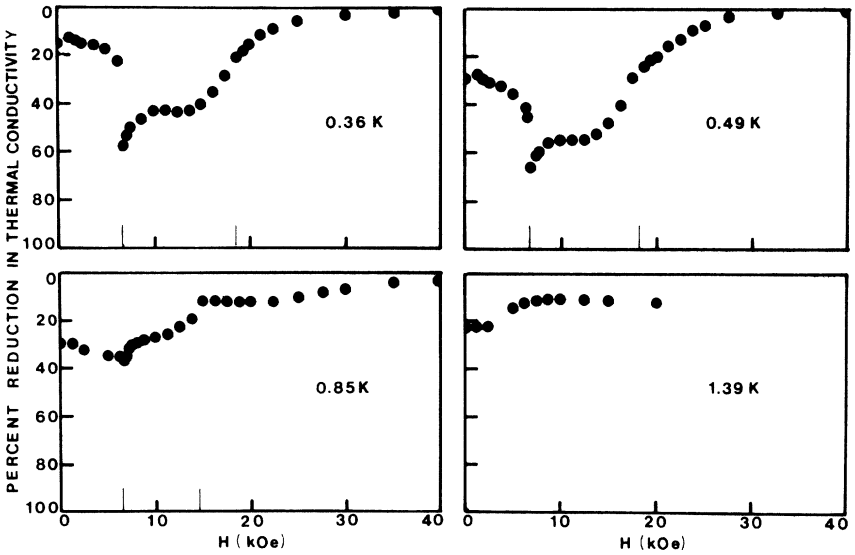

FIG. 3. Magnetic field dependence of the thermal conductivity of $MnCl_2 \cdot 4H_2O$. Note that the magnetic contribution to the thermal resistance persists into the paramagnetic phase.

notes that at the lowest temperatures there is a sharp minimum in the thermal conductivity at the first-order phase boundary between the antiferromagnetic and spin-flop phases. At higher temperatures a strong inflection is seen at this phase transition although not a minimum. At the transition to the paramagnetic phase no distinct structure was observed, the thermal conductivity changing continuously across the phase boundary. Finally, one notes that in the low-temperature, high-field limit the thermal conductivity saturates, demonstrating that effects of magnons have become insignificant.

B. Analysis

The data were analyzed using the two-magnon–one-phonon scattering model developed in the prededing paper.[28] Relaxation times for the phonons, due to magnetic scattering, were obtained with scattering amplitudes for the various processes expressed in terms of gradients of the exchange and anisotropy energies. Thermal conductivities were calculated by the conventional Deybe model for lattice thermal conductivity,[30]

$$K = \frac{k_B}{2\pi^2 v}\left(\frac{k_B T}{\hbar}\right)\int_0^{\Theta/T} \frac{x^4 e^x}{(e^x-1)^2}\,dx \qquad (2)$$

τ is the net relaxation time for the phonons, v is the average sound velocity, and $x = \hbar\omega/k_B T$.

The nonmagnetic contributions to the relaxation time were obtained by applying the Deybe model to the high-field measurements. The average sound velocity $v = 3.0 \times 10^5$ cm/sec was estimated from the specific-heat measurements of Friedberg and Wasscher.[1] The high-field data could be well represented by including contributions from boundary and point defect scattering only, $\tau_0^{-1} = v/0.45 + 6.0 \times 10^{-44}\omega^4$. The boundary scattering length $L = 0.45$ cm agreed to within experimental error with that calculated from the sample's geometry. This calculated thermal conductivity is represented by the curve in Fig. 2.

To model the thermal conductivities in lower fields where effects of magnons are important, the conventional addition of reciprocal relaxation times was used to include the magnon contributions, $\tau^{-1} = \tau_0^{-1} + \tau_m^{-1}(H)$. The exchange and anisotropy from zero-field equilibrium properties[8] were used to evaluate the magnon spectrum. The magnon contribution to the relaxation rate was obtained from the model of the preceding paper.[28] These have the form

$$\tau_{mC}^{-1} = \sum_{ij} [\mathfrak{A}^J(\phi_0 T_{1ij}^5 + \phi_{-k_c} T_{2ij}^J) + \mathfrak{A}^L \phi_0 T_{1ij}^L]^2 k_c^2 n_i n_j n_s^{-1} \qquad (3)$$

and

$$\tau_{mR}^{-1} = [\mathfrak{A}^J(\phi_0 T_{312}^J + \phi_{-k_c} T_{412}^J) + \mathfrak{A}^L \phi_o T_{312}^L]^2 \times k_c^2 (n_1+1) n_2 n_s^{-1} \ , \qquad (4)$$

where s denotes a phonon branch and i and j the magnon branches. k_c is a magnon wave vector on the energy-conservation surface, and the n's are occupation numbers. C processes are those in which a phonon decays into two final-state magnons, and R processes are those in which the phonon scatters a magnon from one state to another. The factors ϕ and T_{mij}^x are tabulated in the preceding paper. The

scattering amplitudes $\mathfrak{A}^J$, and $\mathfrak{A}^L$ are constants arising from modulation of isotropic exchange and single-ion anisotropy, respectively. These were treated as disposable parameters to model the experimental results. It should be noted that Eqs. (3) and (4) contain four relaxation channels for the phonons but only two disposable parameters. Thus, it is not possible to vary the amplitudes of the individual channels independently. The magnetic field dependence arises from the occupation numbers, which are taken as an equilibrium distribution of bosons, and equally importantly from the T^x_{mij} transformation coefficients in the field-induced phases.

Figure 4 shows the temperature dependence of the thermal conductivity in zero field with the T^3 factor of Eq. (2) divided out to faciliate the use of linear scale. The solid curve is obtained using two-magnon–one-phonon interactions as the sole effect of the magnetism. The parameters $\mathfrak{A}^J$ and $\mathfrak{A}^L$ were adjusted to obtain the same maximum reduction in thermal conductivity as observed experimentally. The fit is excellent over the whole range of temperatures except near T_N where renormalization of magnon energies becomes important. It should be emphasized that the temperature at which the maximum thermal resistance occurs is determined by the magnon spectrum and *not* by the disposable coupling constants.[28] The only effect of $\mathfrak{A}^L$ and $\mathfrak{A}^J$ is to set the magnitude of the reduction. Since both exchange modulation and anisotropy modulation have the same temperature and field dependence in the antiferromagnetic phase, it is not possible to determine $\mathfrak{A}^J$ and $\mathfrak{A}^L$ uniquely from this fit alone; there is, in effect, only a single coupling constant in the antiferromagnetic phase.

To apply the two-magnon–one-phonon model to the magnetic field dependence, it is necessary to apportion the scattering between the exchange modulation and anisotropy modulation. This is because of the strong field dependence of the transformation coefficients T^x_{mij} in the field-induced phases. Figures 5 and 6 show the thermal conductivity as a function of field at 0.36 and 0.49 K. The dimensionless field variable h is defined by

$$h = H/H_{AF} \ , \quad H \leq H_{AF} \ ,$$

$$h = 1 + (H - H_{AF})/(H_{FP} - H_{AF}) \ , \quad H_{AF} < H \leq H_{FP} \ ,$$

$$h = 1 + H/H_{FP} \ , \quad H_{FP} < H \ .$$

This is used to take account of the ferromagnetic contributions to the exchange in $MnCl_2 \cdot 4H_2O$ which have not been included in the model. The dashed curves are calculated with all the scattering attributed to exchange modulation with $\mathfrak{A}^J = 1.0$ $(\text{cm}^3\ \text{K/sec}^2)^{1/2}$. This value was determined from the minimum in the temperature dependence of the zero-field data. One notes that the sharp discontinuity at H_{AF} is obtained as is the general shape of the field dependence observed in the field-induced phases. The thermal conductivity in the spin-flop phase rises to a maximum followed by a shallow minimum and a gradual increase until saturation is obtained well into the paramagnetic phase. The model predicts a small anomaly at H_{FP}. This was not

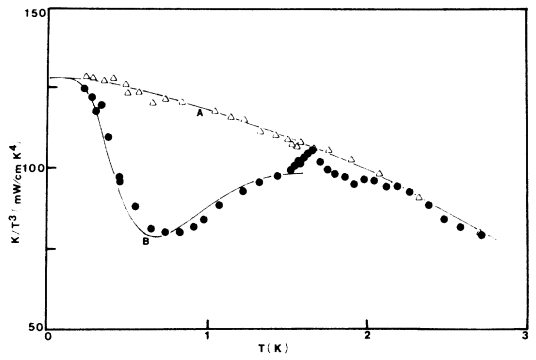

FIG. 4. Temperature dependence of the thermal conductivity divided by T^3. Curve *A* is the least-squares fit to the 40-kOe data (triangles). Curve *B* is a model calculation including two-magnon–one-phonon scattering with the scattering amplitude adjusted to produce the same maximum reduction in thermal conductivity as observed in zero field (circles).

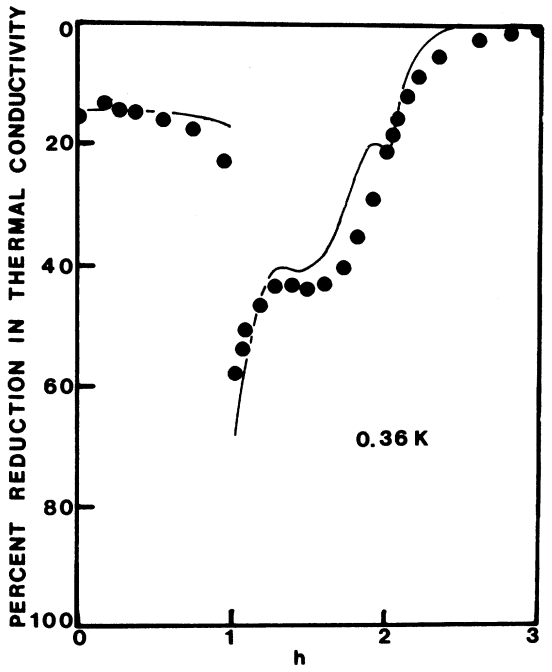

FIG. 5. Magnetic field dependence of the thermal conductivity at 0.36 K. The reduced field h is defined in the text. The curve is the result of the two-magnon–one-phonon calculation.

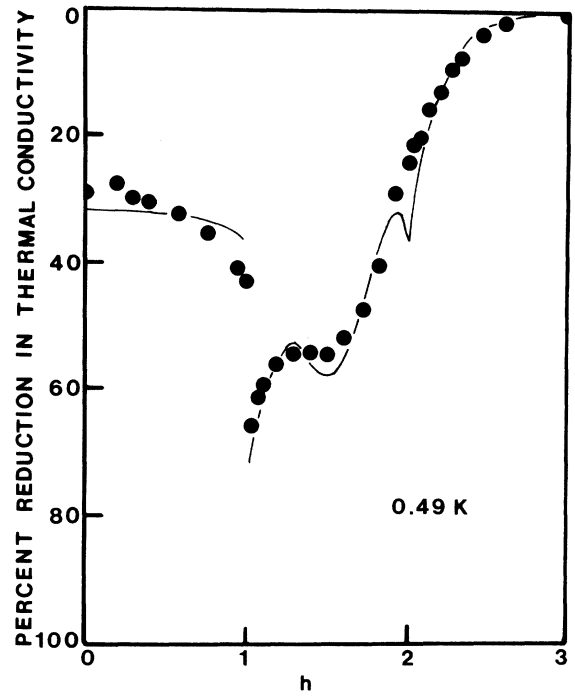

FIG. 6. Magnetic field dependence of the thermal conductivity at 0.49 K. The reduced field h is defined in the text. The curve is the result of the two-magnon–one-phonon calculation.

observed in the present experiments. However, a sharp change in slope near H_{FP} seen in 0.49 K data suggests that the data points were not sufficiently close to H_{FP} to observe the minimum predicted there. The model also predicts that the field dependence in the antiferromagnetic phase should be weaker than observed in these experiments. This additional scattering may be due to the presence of other relaxation channels allowed by magnetic dipole interactions not included in the model or may be an impurity effect.

Extension of the model to high temperatures is limited by magnon renormalization whose effect on the magnetic phase boundaries is substantial even at 0.8 K.[16] This is also seen in the discrepancy between the observed specific heat and that estimated[8] from noninteracting–spin-wave theory. Although renormalization precludes a successful quantitative comparison between theory and experiment, there is still qualitative agreements with the expected effects of two-magnon–one-phonon scattering.

The maximum energy of phonons that can participate in two-magnon–one-phonon processes can be estimated from the experimental values[8] for exchange and anisotropy. In the antiferromagnetic phase this maximum energy is 4.4 K while in the spin-flop phase it is 3.5 K just above the critical field for this transition. At 0.85 K the phonons in the band between 3.5 and 4.4 K are important heat carriers. Thus, there is a tendancy for the thermal conductivity to increase on crossing the phase boundary. For exchange modulation the model predicts a strong minimum near the middle of the spin-flop phase in the absence of renormalization. This is because the increasing energy of the upper branch of magnons increases the maximum energy of phonons that can be scattered by two magnons. This increase will be limited by renormalization resulting in a less pronounced structure. One notes in Fig. 3 that there is an inflection, but no minimum, as the spin-flop phase is crossed at 0.85 K.

In conclusion, it has been found that the major features at low temperatures of the thermal conductivity of $MnCl_2 \cdot 4H_2O$ can be accounted for by intrinsic scattering processes. Two-magnon–one-phonon processes appear to dominate. Earlier attempts to account for these results by invoking one-magnon–one-phonon processes and heat conduction by the magnons were unsuccessful. Both the temperature and magnetic field dependence are obtained from a simple model[28] of the scattering, provided the magnetic field dependence of the transformation to magnon variables is included. Most of the prominent features of both can be obtained using only a single parameter to represent exchange modulation.

ACKNOWLEDGMENT

We are grateful for the hospitality of the Solid State Division, Oak Ridge National Laboratory during the initial stages of this work.

[1]S. A. Friedberg and J. D. Wasscher, Physica (Utrecht) 19, 1072 (1953).
[2]Warren E. Henry, Phys. Rev. 91, 431 (1953).
[3]H. Forstat, G. O. Taylor, and B. R. King, J. Phys. Soc. Jpn. 15, 528 (1960).
[4]H. M. Gijsman, N. J. Poulis, and J. Vanden Handel, Physica (Utrecht) 25, 954 (1959).
[5]W. H. M. Voorhoeve and Z. Dokoupil, Physica (Utrecht) 27, 777 (1961).
[6]M. A. Lasheen, J. Vanden Brock, and C. J. Gorter, Physica (Utrecht) 24, 1061 (1958).
[7]D. G. Kapadmis and R. Hartmans, Physica (Utrecht) 22, 181 (1956).
[8]A. R. Miedema, R. F. Weilinga, and W. J. Huiskamp, Physica (Utrecht) 31, 835 (1969).
[9]John E. Rives, Phys. Rev. 162, 491 (1967).
[10]George S. Dixon and John E. Rives, Phys. Rev. 177, 871 (1969).

[11]J. W. Philp, J. R. Gonano, and E. D. Adams, Phys. Rev. 188, 973 (1969).
[12]J. N. McElearney, H. Forstat, and P. T. Bailey, Phys. Rev. 181, 887 (1969).
[13]W. F. Giauque, R. A. Fisher, E. W. Hornung, and G. E. Brodale, J. Chem. Phys. 53, 1474 (1970).
[14]T. A. Reichert, R. A. Butera, and E. J. Schiller, Phys. Rev. B 1, 4446 (1970).
[15]T. A. Reichert, and W. F. Giauque, J. Chem. Phys. 50, 4205 (1969).
[16]J. E. Rives and V. Benedict, Phys. Rev. B 12, 1908 (1975).
[17]J. E. Rives and D. Walton, Phys. Lett. A 27, 609 (1968).
[18]J. E. Rives, D. Walton, and G. S. Dixon, J. Appl. Phys. 41, 1435 (1970).
[19]M. J. Metcalfe, Phys. Lett. A 36, 373 (1971).
[20]P. Groth, *Chemische Krystallographie* (Englemann, Leipzig, 1908), Vol. I.
[21]C. Delain, C. R. Acad. Sci. 238, 1245 (1954).
[22]J. D. Denney, *Crystal Data,* 2nd ed. (American Crystallographic Association, Washington, D. C., 1963), p. 161.
[23]A. Zalkin, J. D. Forrester, and D. H. Templeton, Inorg. Chem. 3, 529 (1963).
[24]W. E. Gardner, Bull. Am. Phys. Soc. 5, 458 (1960).
[25]W. H. Baur, Inorg. Chem. 4, 1840 (1965).
[26]Z. M. El Saffar and G. M. Brown, Acta Crystallogr. B 27, 777 (1975).
[27]R. F. Altman, S. Spooner, D. P. Landau, and J. E. Rives, Phys. Rev. B 11, 458 (1975).
[28]G. S. Dixon, Phys. Rev. B 21, 2851 (1979) (preceding paper).
[29]G. S. Dixon, Phys. Rev. B 8, 3206 (1973).
[30]R. O. Pohl, Z. Phys. 176, 358 (1963).